

# 1 **Decay of Fc-dependent antibody functions after mild to moderate**

## 2 **COVID-19**

3 Wen Shi Lee<sup>1†</sup>, Kevin John Selva<sup>1†</sup>, Samantha K. Davis<sup>1†</sup>, Bruce D. Wines<sup>2,3,4</sup>, Arnold  
4 Reynaldi<sup>5</sup>, Robyn Esterbauer<sup>1</sup>, Hannah G. Kelly<sup>1</sup>, Ebene R. Haycroft<sup>1</sup>, Hyon-Xhi Tan<sup>1</sup>,  
5 Jennifer A. Juno<sup>1</sup>, Adam K. Wheatley<sup>1,6</sup>, P. Mark Hogarth<sup>2,3,4</sup>, Deborah Cromer<sup>5</sup>, Miles  
6 P. Davenport<sup>5</sup>, Amy W. Chung<sup>1\*</sup>, Stephen J. Kent<sup>1,6,7\*</sup>

7 <sup>†</sup>These authors contributed equally.

8 <sup>1</sup>Department of Microbiology and Immunology, University of Melbourne, at the Peter  
9 Doherty institute for Infection and Immunity, Melbourne, VIC, Australia.

10 <sup>2</sup>Immune Therapies Group, Burnet Institute, Melbourne, VIC, Australia.

11 <sup>3</sup>Department of Clinical Pathology, University of Melbourne, Melbourne, VIC, Australia.

12 <sup>4</sup>Department of Immunology and Pathology, Monash University, Melbourne, VIC,  
13 Australia.

14 <sup>5</sup>Kirby Institute, University of New South Wales, Kensington, NSW, Australia.

15 <sup>6</sup>Australian Research Council Centre for Excellence in Convergent Bio-Nano Science  
16 and Technology, University of Melbourne, Melbourne, VIC, Australia.

17 <sup>7</sup>Melbourne Sexual Health Centre and Department of Infectious Diseases, Alfred  
18 Hospital and Central Clinical School, Monash University, Melbourne, VIC, Australia.

19

20 \*Corresponding authors. Email: [awchung@unimelb.edu.au](mailto:awchung@unimelb.edu.au); [skent@unimelb.edu.au](mailto:skent@unimelb.edu.au).

## 21 **Abstract**

22 The capacity of antibodies to engage with innate and adaptive immune cells via the  
23 Fc region is important in preventing and controlling many infectious diseases, and is  
24 likely critical in SARS-CoV-2 infection. The evolution of such antibodies during  
25 convalescence from COVID-19 is largely unknown. We developed novel assays to  
26 measure Fc-dependent antibody functions against SARS-CoV-2 spike (S)-expressing  
27 cells in serial samples from a cohort of 53 subjects primarily with mild-moderate  
28 COVID-19, out to a maximum of 149 days post-infection. We found that S-specific  
29 antibodies capable of engaging dimeric FcγRIIa and FcγRIIIa decayed linearly over  
30 time. S-specific antibody-dependent cellular cytotoxicity (ADCC) and antibody-  
31 dependent phagocytosis (ADP) activity within plasma declined linearly as well, in line  
32 with the decay of S-specific IgG. Although there was significant decay in S-specific  
33 plasma ADCC and ADP activity, they remained readily detectable by all assays in 94%  
34 of our cohort at the last timepoint studied, in contrast with neutralisation activity which  
35 was only detectable in 70% of our cohort by the last timepoint. Our results suggest  
36 that Fc effector functions such as ADCC and ADP could contribute to the durability of  
37 SARS-CoV-2 immunity, particularly late in convalescence when neutralising  
38 antibodies have waned. Understanding the protective potential of antibody Fc effector  
39 functions is critical for defining the durability of immunity generated by infection or  
40 vaccination.

## 41 **Introduction**

42 Most individuals who recover from COVID-19 develop binding and neutralising  
43 antibody responses against SARS-CoV-2 spike (S) protein (1, 2), with neutralising  
44 antibody responses generally targeted to the receptor-binding domain (RBD) of S (3).  
45 Passive transfer of neutralising monoclonal antibodies (mAbs) can protect animal  
46 models from subsequent SARS-CoV-2 challenge (4-6), suggesting neutralisation is  
47 likely to be a correlate of protection in humans (7). However, the duration of protection  
48 from re-infection in humans conferred by neutralising antibodies is not known. Several  
49 studies now show neutralising antibodies decline rapidly during early convalescence  
50 (2, 8, 9), with the magnitude of the antibody response positively correlating with  
51 disease severity (10, 11). Following mild COVID-19, many subjects mount modest  
52 neutralising antibody responses that decline to undetectable levels within 60 days,  
53 despite the maintenance of S- and RBD-specific IgG binding antibodies (10). Given  
54 that reported cases of SARS-CoV-2 re-infection have been rare to date, it is likely that  
55 immune responses beyond neutralisation contribute to SARS-CoV-2 protective  
56 immunity. Apart from direct virus neutralisation, antibodies can also mediate antiviral  
57 activity such as antibody-dependent cellular cytotoxicity (ADCC) and antibody-  
58 dependent phagocytosis (ADP) by engaging Fc gamma receptors (FcγR) on NK cells  
59 or phagocytes. Fc effector functions contribute to the prevention and control of other  
60 viral infections including HIV-1, influenza and Ebola (12-14). Butler et al. recently  
61 showed that SARS-CoV-2 RBD-specific antibodies within plasma could crosslink Fcγ  
62 receptors, and mediate ADP and antibody-dependent complement deposition (15).  
63 Importantly, two recent challenge studies demonstrated that certain RBD-specific  
64 mAbs rely on Fc effector functions to mediate protection against SARS-CoV-2 in mice  
65 (16, 17).

66

67 We previously reported that binding antibodies to SARS-CoV-2 S exhibit substantially  
68 longer half-lives than the neutralising antibody response (8), suggesting that Fc-  
69 mediated antibody function may extend the protective window beyond that inferred  
70 from neutralising activity alone. At present, analyses of Fc-mediated functions of  
71 SARS-CoV-2 antibodies within COVID-19 convalescent subjects have focussed upon  
72 cross-sectional analyses or short-term longitudinal studies up to 1-2 months post-  
73 symptom onset (15, 18, 19). We extend these findings and analyse Fc effector  
74 functions mediated by S-specific antibodies in a cohort of 53 convalescent individuals  
75 up to 149 days post-symptom onset. We developed novel functional assays using  
76 SARS-CoV-2 S-expressing cells to comprehensively analyse plasma ADCC and ADP  
77 activity against SARS-CoV-2 S. Our results show that plasma ADCC and ADP activity  
78 decay over the first 4 months post-infection, mirroring the decline in S-specific IgG  
79 titres. Importantly, however, S-specific antibodies capable of Fc-mediated antiviral  
80 activity remain readily detectable in almost all donors out to 4 months post-infection,  
81 even in donors whose neutralising antibody responses have waned to undetectable  
82 levels. Consequently, S-specific IgG could potentially mediate Fc-dependent effector  
83 functions that contribute to protection from SARS-CoV-2 infection even in the absence  
84 of plasma neutralising activity.

## 85 **Results**

### 86 **Decay of dimeric FcγR-binding S and RBD-specific antibodies**

87 We collected repeated (2-4) longitudinal samples from a cohort of 53 subjects after  
88 recovery from COVID-19 (Fig 1A, Table S1). The first sample was collected at a  
89 median of 41 days post-symptom onset (IQR 36-48) while the last sample was  
90 collected at a median of 123 days post-symptom onset (IQR 86-135). The engagement  
91 of dimeric recombinant soluble FcγRIIIa and FcγRIIa proteins by antibodies mimics  
92 the immunological synapse required for FcγR activation of innate immune cells, and  
93 is a surrogate measure of ADCC and ADP respectively (20, 21). To determine the  
94 dynamics of Fc-mediated function in plasma samples over time, we measured the  
95 capacity of dimeric FcγRIIIa and FcγRIIa receptors to engage antibodies specific for  
96 SARS-CoV-2 S antigens (trimeric S, S1 or S2 subunits or the RBD; Table S2). Using  
97 mixed-effects modelling, we assessed the fit of single-phase or two-phase decay in  
98 FcγR-binding between the timepoints analysed. We found that dimeric FcγRIIIa  
99 (V158)-binding antibodies against SARS-CoV-2 trimeric S and RBD both had single-  
100 phase decay kinetics with half-lives ( $t_{1/2}$ ) of 175 and 95 days respectively (Fig. 1B-C).  
101 Dimeric FcγRIIa (H131) binding-antibodies against SARS-CoV-2 trimeric S and RBD  
102 also decayed constantly with  $t_{1/2}$  of 175 and 74 days respectively. Kinetics of decay  
103 for dimeric FcγR-binding antibodies against S and RBD for the lower affinity  
104 polymorphisms of FcγRIIIa (F158) and FcγRIIa (R131) were broadly similar to their  
105 higher affinity counterparts (Fig. S1A), with dimeric FcγR-binding antibodies against  
106 RBD decaying faster than for S. Consistent with our previous report that S1-specific  
107 IgG decays faster than S2-specific IgG(8), FcγR binding activity with antibodies  
108 against the S1 subunit decayed faster than that of S2 (FcγRIIIa,  $t_{1/2}$  of 84 vs 227 days;  
109 FcγRIIa,  $t_{1/2}$  of 65 vs 317 days; Fig. S1B).

110

### 111 **Decay of S-specific ADCC**

112 ADCC could play a role in eliminating cells infected with SARS-CoV-2. We generated  
113 Ramos- and A549-derived cell lines as model target cells that stably express  
114 membrane-localised S with either mOrange2 or luciferase reporters (Fig. S2A-B). The  
115 capacity of plasma IgG to recognise S was measured in 36 subjects in our cohort who  
116 had at least 60 days between the first and last visits (median of 89 days between first  
117 and last visits; Table S1) and 8 seronegative controls. Using a Ramos cell line  
118 expressing high levels of S (Ramos S-Orange) (Fig. S2C), we find IgG binding to cell-  
119 surface displayed S proteins decayed significantly between the first and last visits  
120 ( $p < 0.0001$ ; Fig. S2C) with a half-life of 97 days (Fig. S3). These results are consistent  
121 with the decay of S-specific IgG titres we observed previously (8) and the decay of  
122 dimeric FcγR-binding antibodies against S in Fig 1B.

123

124 As a surrogate measure of ADCC, we next used FcγRIIIa reporter cells to quantify the  
125 capacity of S-specific antibodies in plasma to engage cell surface FcγRIIIa and  
126 activate downstream NF-κB signalling (measured by induced nano-luciferase  
127 expression in the FcγRIIIa reporter cells) (Fig. 2A, Fig. S4A). FcγRIIIa activity decayed  
128 significantly over time ( $p < 0.0001$ ; Fig. 2C) with a half-life of 119 days (Fig. S3), and  
129 was correlated with S-specific IgG titres measured using stably transduced cells or by  
130 binding to dimeric FcγRIIIa (Fig. 2D). To confirm antibody recognition could mediate  
131 killing of S-expressing cells, we quantified the loss of cellular luciferase signal in  
132 Ramos S-luciferase target cells in the presence of convalescent plasma and primary  
133 human NK cells (Fig. 2B, Fig. S4B). S-specific ADCC decayed significantly over time

134 ( $p < 0.0001$ ; Fig. 2E) with a half-life of 105 days (Fig. S3), and correlated with both cell-  
135 associated S-specific IgG and dimeric FcγRIIIa-binding antibodies against S (Fig. 2F).

136

### 137 **Decay of S-specific ADP**

138 As has been suggested for SARS-CoV, ADP could play a role in eliminating antibody-  
139 opsonised virions (22). We first used a well-established ADP assay (23) to measure  
140 antibody-mediated uptake of S-conjugated fluorescent beads into THP-1 monocytes  
141 (Fig. 3A; gating in Fig. S5A-B and optimisation in Fig. S6A-C). ADP of S-conjugated  
142 beads was detected in all 36 subjects at the first time point studied but decayed  
143 significantly over time ( $p < 0.0001$ ; Fig. 3C) with a half-life of 263 days (Fig. S3). ADP  
144 of S-conjugated beads correlated with cell-associated S-specific IgG and S-specific  
145 dimeric FcγRIIIa-binding antibodies (Fig. 3D).

146

147 In addition to uptake of antibody-opsonised virions, phagocytes could also potentially  
148 mediate clearance of infected cells expressing SARS-CoV-2 S on the cell surface.  
149 THP-1 cells have been shown to mediate both trogocytosis (sampling of plasma  
150 membrane fragments from target cells that can lead to cell death) and phagocytosis  
151 via antibody Fc-FcγR interactions with target cells (24-26). As such, we measured the  
152 FcγR-dependent association of THP-1 cells with Ramos S-orange cells following  
153 incubation with plasma from convalescent individuals or uninfected controls (Fig. 3B;  
154 gating in Fig. S5C and optimisation in Fig. S6D-F). Association of THP-1 cells with  
155 Ramos S-orange cells was detected in all subjects at the first time point but decayed  
156 significantly over time ( $p < 0.0001$ ; Fig. 3E) with a half-life of 351 days (Fig. S3),  
157 correlating with IgG binding to cell-associated S and S-specific dimeric FcγRIIIa-  
158 binding antibodies (Fig. 3F).

159

## 160 **Cross-reactivity with HCoV S-specific antibodies**

161 Cross-reactive antibodies between endemic human coronaviruses (HCoV) and SARS-  
162 CoV-2 have been widely reported (27, 28), suggesting past exposure to HCoVs may  
163 prime ADCC and ADP immunity against SARS-CoV-2. In addition, several studies  
164 have shown back-boosting of antibodies against endemic human coronaviruses  
165 (HCoV) following infection with SARS-CoV-2 (29, 30), likely due to the recall of pre-  
166 existing B cell responses against conserved regions of S. We thus determined whether  
167 IgG antibodies against S from four HCoV strains (OC43, HKU1, 229E and NL63)  
168 (Table S2) were boosted in COVID-19 convalescent subjects compared to uninfected  
169 healthy controls. We found that COVID-19 convalescent subjects had increased IgG  
170 antibodies against S from the betacoronaviruses OC43 and HKU1 (that are more  
171 closely related to SARS-CoV-2) at the first timepoint sampled compared to uninfected  
172 controls (Fig S7), while there was no difference in IgG levels against S from the  
173 alphacoronaviruses 229E and NL63. Correspondingly, the elevated IgG against OC43  
174 and HKU1 S decayed over time while IgG against 229E and NL63 S remained stable  
175 (Fig 4A). We then measured whether dimeric FcγR-binding antibodies against HCoV  
176 S antigens in COVID-19 convalescent individuals declined over time. Dimeric FcγR-  
177 binding antibodies against OC43 and HKU1 S antigens were much higher in COVID-  
178 19 convalescent individuals than in healthy controls and decayed more rapidly over  
179 time compared to that against 229E and NL63 (Fig. 4A, Fig S8A-C). While there was  
180 an overall decay of dimeric FcγR-binding antibodies against OC43 S (FcγRIIIa  $t_{1/2}$  =  
181 224, FcγRIIIa  $t_{1/2}$  = 171 days), this was largely due to a decay in antibodies against the  
182 more conserved S2 subunit (FcγRIIIa  $t_{1/2}$  = 229, FcγRIIIa  $t_{1/2}$  = 179 days) as FcγR-  
183 binding antibodies against the S1 subunit were not boosted and did not change



184 substantially over time (Fig. 4B-C). This was also the case for HKU1, where dimeric  
185 FcγR-binding antibodies against S decayed over time but antibodies against the S1  
186 subunit did not change (Fig S8A).

187

### 188 **Decay kinetics of S-specific antibodies, neutralisation and Fc effector functions**

189 To compare the decay kinetics of S-specific antibodies, neutralisation and Fc effector  
190 functions, we plotted the best fit decay slopes over time as a percentage of the  
191 response measured at timepoint 1 (Fig. 5A). The best-fit decay slopes of S-specific  
192 IgG and plasma neutralisation titres were obtained from a previous dataset that  
193 encompass the same subjects analysed for dimeric FcγR-binding antibodies and Fc  
194 effector functions (8) (Fig. S3). The general decline in plasma S-specific IgG titres and  
195 dimeric FcγR-binding activity was similarly reflected in reductions in Fc effector  
196 functions during convalescence from COVID-19. Importantly, Fc effector functions at  
197 the last timepoint sampled were still readily detectable above baseline activity  
198 observed in uninfected controls (97% for FcγRIIIa activation, 94% for ADCC, 100% for  
199 ADP and 100% for THP-1 association). This contrasted with plasma neutralisation  
200 activity, which was detectable above background for only 70% of subjects (Fig. 5B).  
201 The longer persistence of S-specific IgG and dimeric FcγR-binding antibodies against  
202 S has important implications as they may contribute to protection from SARS-CoV-2  
203 infection following the decline of neutralising antibodies.

## 204 Discussion

205 Using a multiplex bead array and novel assays measuring Fc effector functions against  
206 SARS-CoV-2 S, we find that FcγR-binding, ADCC and ADP activities of S-specific  
207 antibodies decay during convalescence from COVID-19. The decline of plasma ADCC  
208 and ADP activity correlated with the decay of S-specific IgG and FcγR-binding  
209 antibodies. Importantly, Fc effector functions were readily detectable above uninfected  
210 controls in 94% of subjects for all assays at the last timepoint sampled, in sharp  
211 contrast with neutralisation activity, which remained detectable above background for  
212 only 70% of subjects. While neutralising antibodies are likely to form a correlate of  
213 protection for SARS-CoV-2 (7), several studies find that neutralising antibodies in  
214 convalescent donors with mild COVID-19 wane rapidly (2, 8, 9). The rapid decline of  
215 plasma neutralisation activity in the early weeks following infection could potentially be  
216 explained by the rapid decline of plasma IgM and IgA titres against S and RBD (19,  
217 31), which substantially contribute to neutralisation of SARS-CoV-2 (32-34). Given the  
218 relative scarcity of re-infection cases reported to date, it is likely that immune  
219 responses beyond neutralisation, including antibody Fc effector functions and T cell  
220 responses, contribute to long-term protection from SARS-CoV-2. Indeed, a recent  
221 study demonstrated that cellular immunity in convalescent macaques, mainly CD8<sup>+</sup> T  
222 cells, contribute to protection against re-challenge after neutralising antibodies have  
223 waned (22, 35).

224

225 Our results demonstrate that FcγR-binding antibodies against betacoronaviruses  
226 OC43 and HKU1 are much higher in COVID-19 convalescent individuals compared to  
227 uninfected controls. This could either be due to the back-boosting of pre-existing HCoV  
228 antibodies that are cross-reactive with SARS-CoV-2 (27, 28), or the *de novo*

229 generation of SARS-CoV-2 antibodies that are cross-reactive with conserved HCoV  
230 epitopes. Cross-reactive S antibodies were largely directed against the more  
231 conserved S2 subunit, in line with other reports (27, 28). A recent study found cross-  
232 reactive binding and neutralising antibodies against SARS-CoV-2 S2 in uninfected  
233 children and adolescents (27), suggesting prior infections with OC43 or HKU1 can  
234 elicit cross-reactive antibodies against the S2 subunit of SARS-CoV-2 S. These  
235 findings raise the interesting question of whether cross-reactive antibodies are  
236 recalled rapidly during early SARS-CoV-2 infection and can contribute to Fc effector  
237 functions against conserved epitopes within the S2 subunit. The presence of cross-  
238 reactive S2-specific antibodies capable of mediating Fc effector functions in early  
239 infection could potentially ameliorate disease symptoms and severity. Follow-up  
240 studies to dissect the influence of S1 or S2 antibody epitope localisation on FcγR  
241 engagement and the impact on Fc effector functions are also warranted.

242

243 Initial concerns for antibody-dependent enhancement (ADE) of COVID-19 were driven  
244 by the reported association of higher SARS-CoV-2 antibody titres with severe disease  
245 (36). However, this could simply be the result of prolonged antigen exposure due to  
246 higher viral loads. Importantly, Zohar et al. showed that in subjects with severe COVID-  
247 19, those who survived had higher levels of S-specific antibodies and Fc-mediated  
248 effector functions compared to those who died (31). Notably, numerous trials of  
249 convalescent plasma (CP) therapy for COVID-19 have been safely conducted (37-39),  
250 with no enhancement of disease reported to date (40-42). Since RBD-specific IgG1  
251 antibodies in severe COVID-19 are more likely to have afucosylated Fc regions and  
252 trigger hyper-inflammatory responses from monocytes and macrophages (43, 44),  
253 there could be implications for ADE in people who are re-infected with SARS-CoV-2

254 after initial neutralising antibodies have waned but non-neutralising antibodies remain.  
255 Excessive Fc-mediated effector functions and immune complex formation in the  
256 absence of neutralisation could potentially trigger a hyper-inflammatory response and  
257 lead to ADE of disease, as observed for RSV and measles infections (45, 46). While  
258 ADE during re-infection remains only a theoretical risk, there have been two reported  
259 cases of re-infection where the second infection resulted in worse disease (47, 48).  
260 However, antibody levels after the first infection were not measured for one case (47)  
261 and only IgM was detectable after the first infection for the second case (48), arguing  
262 against Fc-mediated effector functions as the cause of increased pathogenicity.  
263  
264 Overall, we find that FcγR-binding, ADCC and ADP antibody functions decay following  
265 recovery from COVID-19 at a slower rate than serum neutralisation activity,  
266 suggesting non-neutralising antibody responses elicited by infection or vaccination  
267 may contribute to durable protection against SARS-CoV-2.

## 268 **Materials and methods**

### 269 **Cohort recruitment and sample collection**

270 People who recovered from COVID-19 and healthy controls were recruited to provide  
271 serial whole blood samples. Convalescent donors either had a PCR+ test during early  
272 infection or clear exposure to SARS-CoV-2, and were confirmed to have SARS-CoV-  
273 2 S- and RBD-specific antibodies via ELISA as previously reported (1).  
274 Contemporaneous uninfected controls who did not experience any COVID-19  
275 symptoms were also recruited and confirmed to be seronegative via ELISA. For all  
276 subjects, whole blood was collected with sodium heparin or lithium heparin  
277 anticoagulant. The plasma fraction was then collected and stored at -80°C. A subset  
278 of 36 donors with at least 60 days between the first and last visits were chosen to  
279 proceed with the more labour-intensive functional ADCC and ADP assays. Plasma  
280 was heat-inactivated at 56°C for 30 minutes prior to use in functional assays.  
281 Characteristics of the COVID-19 convalescent and uninfected donors are described  
282 in Table S1. The study protocols were approved by the University of Melbourne  
283 Human Research Ethics Committee (#2056689). All subjects provided written  
284 informed consent in accordance with the Declaration of Helsinki.

285

### 286 **Luminex bead-based multiplex assay**

287 As previously described (49), a custom multiplex bead array was designed and  
288 coupled with SARS-CoV-2 S trimer, S1 subunit (Sino Biological), S2 subunit (ACRO  
289 Biosystems) and RBD (BEI Resources), as well as HCoV (OC43, HKU1, 229E, NL63)  
290 S (Sino Biological) (Table S2). Tetanus toxoid (Sigma-Aldrich), influenza  
291 hemagglutinin (H1Cal2009; Sino Biological) and SIV gp120 (Sino Biological) were also  
292 included in the assay as positive and negative controls respectively. Antigens were

293 covalently coupled to magnetic carboxylated beads (Bio Rad) using a two-step  
294 carbodiimide reaction and blocked with 0.1% BSA, before being resuspended and  
295 stored in PBS 0.05% sodium azide till use.

296

297 Using the coupled beads, a custom CoV multiplex assay was formed to investigate  
298 the dimeric recombinant soluble FcγR-binding capacity of pathogen-specific  
299 antibodies present in COVID-19 convalescent plasma samples and uninfected  
300 controls (49). Briefly, 20μl of working bead mixture (1000 beads per bead region) and  
301 20μl of diluted plasma (final dilution 1:200) were added per well and incubated  
302 overnight at 4°C on a shaker. Different detectors were used to assess pathogen-  
303 specific antibodies. Single-step detection was done using phycoerythrin (PE)-  
304 conjugated mouse anti-human pan-IgG (Southern Biotech; 1.3μg/ml, 25μl/well). For  
305 the detection of FcγR-binding, recombinant soluble FcγR dimers (higher affinity  
306 polymorphisms FcγRIIIa-V158 and FcγRIIa-H131, lower affinity polymorphisms  
307 FcγRIIIa-F158 and FcγRIIa-R131; 1.3μg/ml, 25μl/well) were first added to the beads,  
308 washed, followed by the addition of streptavidin R-PE (Thermo Fisher Scientific).  
309 Assays were read on the Flexmap 3D and performed in duplicates.

310

### 311 **Cell lines**

312 As target cells for the functional antibody assays, Ramos and A549 cells stably  
313 expressing full-length SARS-CoV-2 S and the reporter proteins mOrange2 or  
314 luciferase were generated by lentiviral transduction (Fig. S2A). To stain for S-  
315 expression, transduced cells were incubated with convalescent plasma (1:100 dilution)  
316 prior to staining with a secondary mouse anti-human IgG-APC antibody (1:200 dilution;  
317 clone HP6017, BioLegend). S-luciferase cells were bulk sorted on high S expression

318 while S-orange cells were bulk sorted on high S- and mOrange2-expression. Following  
319 a week of outgrowth, the bulk sorted cells were single-cell sorted to obtain clonal  
320 populations of S-orange and S-luciferase cells (Fig. S2B). The Ramos cell lines were  
321 grown in complete RPMI medium (10% fetal calf serum (FCS) with 1% penicillin  
322 streptomycin glutamine (PSG)) while the A549 cell lines were grown in complete  
323 DMEM medium (10% FCS with 1% PSG).

324

325 FcγRIIIa-NF-κB-RE nanoluciferase reporter cells were used as effector cells for the  
326 FcγRIIIa activation assay. IIA1.6 cells expressing the Fc receptor gamma subunit  
327 (FcR-γ) were maintained in RPMI containing 10% FCS, 2.5 mM L-glutamine, 55 μM  
328 2-mercaptoethanol, 100 units penicillin and 100 units streptomycin (Sigma Aldrich).  
329 These were further transduced as described previously (50) using a FcγRIIIa V158  
330 cDNA in pMX-neo and the packaging line Phoenix. IIA1.6/FcR-γ/FcγRIIIa V158 cells  
331 were transfected with a NF-κB response element driven nanoluciferase (NanoLuc)  
332 reporter construct (pNL3.2.NF-κB-RE[NlucP/NF-κB-RE/Hygro] (Promega) by  
333 nucleofection (Amaxa Kit T, Lonza) and selected in the presence of 200 μg/ml  
334 hygromycin. Reporter cells were maintained in media containing 400 μg/ml neomycin  
335 and 50 μg/ml hygromycin (ThermoFisher).

336

337 THP-1 monocytes (ATCC) were cultured in complete RPMI medium and maintained  
338 below a cell density of  $0.3 \times 10^6$ /ml. Flow cytometry was used to confirm stable  
339 expression of FcγRIIIa (CD32), FcγRI (CD64) and FcαR (CD89) on THP-1 monocytes  
340 prior to use in assays.

341

342 **FcγRIIIa activation assay**

343 A549 S-orange cells were plated ( $2 \times 10^5$ /ml, 100  $\mu$ l/well) in 96-well white flat-bottom  
344 plates (Corning). The next day, COVID-19 convalescent and uninfected plasma were  
345 serially diluted and 50  $\mu$ l aliquots transferred to the aspirated A549 S-orange cells and  
346 incubated at 37°C, 60 min, 5% CO<sub>2</sub>. Unbound antibody was removed by aspirating the  
347 wells and refilling with RPMI (200  $\mu$ l) four times. Fc $\gamma$ RIIIa-NF- $\kappa$ B-RE nanoluciferase  
348 reporter cells ( $4 \times 10^5$ /ml, 50  $\mu$ l/well) were added to the aspirated wells containing the  
349 opsonised A549 S-orange cells. After incubation (37°C, 4h, 5%CO<sub>2</sub>) cells were lysed  
350 by adding 50  $\mu$ l/well of 10 mM Tris-pH 7.4, containing 5 mM EDTA, 0.5 mM DTT, 0.2%  
351 Igepal CA-630 (Sigma Aldrich), and Nano-Glo luciferase assay substrate (1:1000).  
352 Induction of nanoluciferase was measured using a 1s read on a Clariostar Optima  
353 plate reader (BMG Labtech) with background luminescence from control wells without  
354 agonist subtracted from test values.

355

### 356 **Luciferase-based ADCC assay**

357 A luciferase-based ADCC assay was performed to examine ADCC against S-  
358 expressing cells. NK cells from healthy donors were first enriched from freshly isolated  
359 PBMCs using the EasySep Human NK Cell Enrichment Kit (Stemcell Technologies).  
360 In a 96-well V-bottom cell culture plate, purified NK cells (20,000/well) were mixed with  
361 Ramos S-luciferase cells (5,000/well) in the presence or absence of plasma from  
362 convalescent or uninfected donors at 1:100, 1:400 and 1:1600 dilutions. Each  
363 condition was tested in duplicate and “no plasma” and “target cell only” controls were  
364 included. Cells were centrifuged at 250g for 4 min prior to a 4-hour incubation at 37°C  
365 with 5% CO<sub>2</sub>. Cells were then washed with PBS and lysed with 25 $\mu$ l of passive lysis  
366 buffer (Promega). Cell lysates (20 $\mu$ l) were transferred to a white flat-bottom plate and  
367 developed with 30 $\mu$ l of britelite plus luciferase reagent (Perkin Elmer). Luminescence



368 was read using a FLUOstar Omega microplate reader (BMG Labtech). The relative  
369 light units (RLU) measured were used to calculate %ADCC with the following formula:  
370 (“no plasma control” – “plasma sample”) ÷ “target cell only control” × 100. For each  
371 plasma sample, %ADCC was plotted against  $\log_{10}(\text{plasma dilution}^{-1})$  and the area  
372 under curve (AUC) was calculated using Graphpad Prism.

373

#### 374 **Bead-based THP-1 ADP assay**

375 To examine ADP mediated by COVID-19 convalescent plasma, a previously published  
376 bead-based ADP assay was adapted for use in the context of SARS-CoV-2 (23).  
377 SARS-CoV-2 S trimer was biotinylated using EZ-Link Sulfo-NHS-LC biotinylation kit  
378 (Thermo Scientific) with 20mmol excess according to manufacturer’s instructions and  
379 buffer exchanged using 30kDa Amicon centrifugal filters (EMD millipore) to remove  
380 free biotin. The binding sites of 1µm fluorescent NeutrAvidin Fluospheres beads  
381 (Invitrogen) were coated with biotinylated S at a 1:3 ratio overnight at 4°C. S-  
382 conjugated beads were washed four times with 2% BSA/PBS to remove excess  
383 antigen and incubated with plasma (1:100 dilution) for 2 hours at 37°C in a 96-well U-  
384 bottom plate (see Fig. S6 for optimisation). THP-1 monocytes (10,000/well) were then  
385 added to opsonized beads and incubated for 16 hours under cell culture conditions.  
386 Cells were fixed with 2% formaldehyde and acquired on a BD LSR Fortessa with a  
387 HTS. The data was analyzed using FlowJo 10.7.1 (see Fig. S5 for gating strategy) and  
388 a phagocytosis score was calculated as previously described (51) using the formula:  
389  $(\% \text{bead-positive cells} \times \text{mean fluorescent intensity}) / 10^3$ . To account for non-specific  
390 uptake of S-conjugated beads, the phagocytosis scores for each plasma sample were  
391 subtracted with that of the “no plasma” control.

392

### 393 **Cell-based THP-1 association assay**

394 To assess the capacity of THP-1 monocytes to associate with S-expressing target  
395 cells via Ab-FcγR interactions, an assay using THP-1 cells as effectors and Ramos S-  
396 orange cells as targets was performed. THP-1 monocytes were first stained with  
397 CellTrace™ Violet (CTV) (Life Technologies) as per manufacturer's instructions. In a  
398 96-well V-bottom cell culture plate, Ramos S-orange cells (10,000/well) were  
399 incubated with plasma from convalescent or uninfected donors (1:2700 dilution) for 30  
400 minutes (see Fig. S6 for optimisation). Opsonised Ramos S-orange cells were then  
401 washed prior to co-culture with CTV-stained THP-1 monocytes (10,000/well) for 1 hour  
402 at 37°C with 5% CO<sub>2</sub>. After the incubation, cells were washed with PBS, fixed with 2%  
403 formaldehyde and acquired using the BD LSR Fortessa with a high-throughput  
404 sampler attachment (HTS). The data was analyzed using FlowJo 10.7.1 (see Fig. S5  
405 for gating strategy). The percentage of Ramos S-orange cells associated with THP-1  
406 monocytes (% association) was measured for each plasma sample and background-  
407 subtracted with the “no plasma” control.

408

### 409 **Decay rate estimation**

410 The decay rate was estimated by fitting a linear mixed effect model for each response  
411 variable ( $y_{ij}$  for subject  $i$  at timepoint  $j$ ) as a function of days post-symptom onset and  
412 assay replicate (as a binary categorical variable). The model can be written as below:

413  $y_{ij} = \beta_0 + b_{0i} + \beta_1 R_{ij} + \beta_2 t_{ij} + b_{2i} t_{ij}$  – for a model with a single slope; and

414  $y_{ij} = \beta_0 + b_{0i} + \beta_1 R_{ij} + \beta_2 t_{ij} + b_{2i} t_{ij} + \beta_3 s_{ij} + b_{3i} s_{ij}$  – for a model with two different  
415 slopes, in which:

416 
$$s_{ij} = \begin{cases} 0, & t_{ij} < T_0 \\ t_{ij} - T_0, & t_{ij} \geq T_0. \end{cases}$$

417 The parameter  $\beta_0$  is a constant (intercept), and  $b_{0i}$  is a subject-specific adjustment to  
418 the overall intercept. The slope parameter  $\beta_2$  is a fixed effect to capture the decay  
419 slope before  $T_0$  (as a fixed parameter, 70 days); which also has a subject-specific  
420 random effect  $b_{2i}$ . To fit a model with two different decay rates, an extra parameter  $\beta_3$   
421 (with a subject-specific random effect  $b_{3i}$ ) was added to represent the difference  
422 between the two slopes. Assay variability between replicates (only for HCoV response  
423 variables) was modelled as a single fixed effect  $\beta_1$ , in which we coded the replicate as  
424 a binary categorical variable  $R_{ij}$ . The random effect was assumed to be normally  
425 distributed with zero mean and variance  $\delta$ .

426

427 We fitted the model to log-transformed data of various response variables, and we  
428 censored the data from below if it was less than the threshold for detection. The  
429 response variables had background levels subtracted by taking the mean of all the  
430 background values, and the threshold for detection was set at two standard deviations  
431 of the background responses. The model was fitted by using *lme4* library in *R*, using  
432 the ML algorithm to fit for the fixed effects. We also tested if the response variables  
433 can be fitted better by using a single or two different decay slopes (likelihood ratio test  
434 – based on the likelihood value and the difference in the number of parameters). These  
435 analyses were carried out in *R: A language and environment for statistical computing*  
436 version 4.0.2.

437

## 438 **Statistics**

439 Statistical analyses were performed with Graphpad Prism 8. Correlations between  
440 functional ADCC and ADP responses with cell-associated S-specific IgG and FcγR-  
441 binding S-specific antibodies were assessed using the non-parametric Spearman test.

442 Comparisons of functional ADCC and ADP responses between first and last visits  
443 were performed using the Wilcoxon signed-rank test. Comparisons between  
444 uninfected individuals and COVID-19 convalescent individuals were performed using  
445 the Mann-Whitney test.

## 446 References

- 447 1. J. A. Juno, H. X. Tan, W. S. Lee, A. Reynaldi, H. G. Kelly, K. Wragg, R.  
448 Esterbauer, H. E. Kent, C. J. Batten, F. L. Mordant, N. A. Gherardin, P. Pymm,  
449 M. H. Dietrich, N. E. Scott, W. H. Tham, D. I. Godfrey, K. Subbarao, M. P.  
450 Davenport, S. J. Kent, A. K. Wheatley, Humoral and circulating follicular helper  
451 T cell responses in recovered patients with COVID-19. *Nat Med* **26**, 1428-1434  
452 (2020).
- 453 2. A. Wajnberg, F. Amanat, A. Firpo, D. R. Altman, M. J. Bailey, M. Mansour, M.  
454 McMahon, P. Meade, D. R. Mendu, K. Muellers, D. Stadlbauer, K. Stone, S.  
455 Strohmeier, V. Simon, J. Aberg, D. L. Reich, F. Krammer, C. Cordon-Cardo,  
456 Robust neutralizing antibodies to SARS-CoV-2 infection persist for months.  
457 *Science*, (2020).
- 458 3. L. Piccoli, Y. J. Park, M. A. Tortorici, N. Czudnochowski, A. C. Walls, M.  
459 Beltramello, C. Silacci-Fregni, D. Pinto, L. E. Rosen, J. E. Bowen, O. J. Acton,  
460 S. Jaconi, B. Guarino, A. Minola, F. Zatta, N. Sprugasci, J. Bassi, A. Peter, A.  
461 De Marco, J. C. Nix, F. Mele, S. Jovic, B. F. Rodriguez, S. V. Gupta, F. Jin, G.  
462 Piumatti, G. Lo Presti, A. F. Pellanda, M. Biggiogero, M. Tarkowski, M. S.  
463 Pizzuto, E. Cameroni, C. Havenar-Daughton, M. Smithey, D. Hong, V. Lepori,  
464 E. Albanese, A. Ceschi, E. Bernasconi, L. Elzi, P. Ferrari, C. Garzoni, A. Riva,  
465 G. Snell, F. Sallusto, K. Fink, H. W. Virgin, A. Lanzavecchia, D. Corti, D. Veessler,  
466 Mapping Neutralizing and Immunodominant Sites on the SARS-CoV-2 Spike  
467 Receptor-Binding Domain by Structure-Guided High-Resolution Serology. *Cell*  
468 **183**, 1024-1042 e1021 (2020).
- 469 4. T. F. Rogers, F. Zhao, D. Huang, N. Beutler, A. Burns, W. T. He, O. Limbo, C.  
470 Smith, G. Song, J. Woehl, L. Yang, R. K. Abbott, S. Callaghan, E. Garcia, J.  
471 Hurtado, M. Parren, L. Peng, S. Ramirez, J. Ricketts, M. J. Ricciardi, S. A.  
472 Rawlings, N. C. Wu, M. Yuan, D. M. Smith, D. Nemazee, J. R. Teijaro, J. E.  
473 Voss, I. A. Wilson, R. Andrabi, B. Briney, E. Landais, D. Sok, J. G. Jardine, D.  
474 R. Burton, Isolation of potent SARS-CoV-2 neutralizing antibodies and  
475 protection from disease in a small animal model. *Science*, (2020).
- 476 5. L. Liu, P. Wang, M. S. Nair, J. Yu, M. Rapp, Q. Wang, Y. Luo, J. F. Chan, V.  
477 Sahi, A. Figueroa, X. V. Guo, G. Cerutti, J. Bimela, J. Gorman, T. Zhou, Z. Chen,  
478 K. Y. Yuen, P. D. Kwong, J. G. Sodroski, M. T. Yin, Z. Sheng, Y. Huang, L.  
479 Shapiro, D. D. Ho, Potent neutralizing antibodies against multiple epitopes on  
480 SARS-CoV-2 spike. *Nature* **584**, 450-456 (2020).
- 481 6. A. Baum, D. Ajithdoss, R. Copin, A. Zhou, K. Lanza, N. Negron, M. Ni, Y. Wei,  
482 K. Mohammadi, B. Musser, G. S. Atwal, A. Oyejide, Y. Goetz-Gazi, J. Dutton,  
483 E. Clemmons, H. M. Staples, C. Bartley, B. Klaffke, K. Alfson, M. Gazi, O.  
484 Gonzalez, E. Dick, Jr., R. Carrion, Jr., L. Pessaint, M. Porto, A. Cook, R. Brown,  
485 V. Ali, J. Greenhouse, T. Taylor, H. Andersen, M. G. Lewis, N. Stahl, A. J.  
486 Murphy, G. D. Yancopoulos, C. A. Kyratsous, REGN-COV2 antibodies prevent  
487 and treat SARS-CoV-2 infection in rhesus macaques and hamsters. *Science*,  
488 (2020).
- 489 7. A. Addetia, K. H. D. Crawford, A. Dingens, H. Zhu, P. Roychoudhury, M. L.  
490 Huang, K. R. Jerome, J. D. Bloom, A. L. Greninger, Neutralizing Antibodies  
491 Correlate with Protection from SARS-CoV-2 in Humans during a Fishery Vessel  
492 Outbreak with a High Attack Rate. *J Clin Microbiol* **58**, (2020).
- 493 8. A. K. Wheatley, J. A. Juno, J. J. Wang, K. J. Selva, A. Reynaldi, H.-X. Tan, W.  
494 S. Lee, K. M. Wragg, H. G. Kelly, R. Esterbauer, S. K. Davis, H. E. Kent, F. L.

- 495 Mordant, T. E. Schlub, D. L. Gordon, D. S. Khoury, K. Subbarao, D. Cromer, T.  
496 P. Gordon, A. W. Chung, M. P. Davenport, S. J. Kent, Evolution of immunity to  
497 SARS-CoV-2. *medRxiv*, 2020.2009.2009.20191205 (2020).
- 498 9. K. H. D. Crawford, A. S. Dingens, R. Eguia, C. R. Wolf, N. Wilcox, J. K. Logue,  
499 K. Shuey, A. M. Casto, B. Fiala, S. Wrenn, D. Pettie, N. P. King, A. L. Greninger,  
500 H. Y. Chu, J. D. Bloom, Dynamics of neutralizing antibody titers in the months  
501 after SARS-CoV-2 infection. *J Infect Dis*, (2020).
- 502 10. J. Seow, C. Graham, B. Merrick, S. Acors, S. Pickering, K. J. A. Steel, O.  
503 Hemmings, A. O'Byrne, N. Kouphou, R. P. Galao, G. Betancor, H. D. Wilson,  
504 A. W. Signell, H. Winstone, C. Kerridge, I. Huettner, J. M. Jimenez-Guardeno,  
505 M. J. Lista, N. Temperton, L. B. Snell, K. Bisnauthsing, A. Moore, A. Green, L.  
506 Martinez, B. Stokes, J. Honey, A. Izquierdo-Barras, G. Arbane, A. Patel, M. K.  
507 I. Tan, L. O'Connell, G. O'Hara, E. MacMahon, S. Douthwaite, G. Nebbia, R.  
508 Batra, R. Martinez-Nunez, M. Shankar-Hari, J. D. Edgeworth, S. J. D. Neil, M.  
509 H. Malim, K. J. Doores, Longitudinal observation and decline of neutralizing  
510 antibody responses in the three months following SARS-CoV-2 infection in  
511 humans. *Nat Microbiol*, (2020).
- 512 11. A. T. Huang, B. Garcia-Carreras, M. D. T. Hitchings, B. Yang, L. C. Katzelnick,  
513 S. M. Rattigan, B. A. Borgert, C. A. Moreno, B. D. Solomon, L. Trimmer-Smith,  
514 V. Etienne, I. Rodriguez-Barraquer, J. Lessler, H. Salje, D. S. Burke, A.  
515 Wesolowski, D. A. T. Cummings, A systematic review of antibody mediated  
516 immunity to coronaviruses: kinetics, correlates of protection, and association  
517 with severity. *Nat Commun* **11**, 4704 (2020).
- 518 12. S. Bournazos, F. Klein, J. Pietzsch, M. S. Seaman, M. C. Nussenzweig, J. V.  
519 Ravetch, Broadly neutralizing anti-HIV-1 antibodies require Fc effector  
520 functions for in vivo activity. *Cell* **158**, 1243-1253 (2014).
- 521 13. D. J. DiLillo, P. Palese, P. C. Wilson, J. V. Ravetch, Broadly neutralizing anti-  
522 influenza antibodies require Fc receptor engagement for in vivo protection. *J*  
523 *Clin Invest* **126**, 605-610 (2016).
- 524 14. S. Bournazos, D. J. DiLillo, A. J. Goff, P. J. Glass, J. V. Ravetch, Differential  
525 requirements for FcγR engagement by protective antibodies against  
526 Ebola virus. *Proc Natl Acad Sci U S A* **116**, 20054-20062 (2019).
- 527 15. S. E. Butler, A. R. Crowley, H. Natarajan, S. Xu, J. A. Weiner, J. Lee, W. F.  
528 Wieland-Alter, R. I. Connor, P. F. Wright, M. E. Ackerman, Features and  
529 Functions of Systemic and Mucosal Humoral Immunity Among SARS-CoV-2  
530 Convalescent Individuals. *medRxiv*, 2020.2008.2005.20168971 (2020).
- 531 16. A. Schafer, F. Muecksch, J. C. C. Lorenzi, S. R. Leist, M. Cipolla, S. Bournazos,  
532 F. Schmidt, R. M. Maison, A. Gazumyan, D. R. Martinez, R. S. Baric, D. F.  
533 Robbiani, T. Hatziioannou, J. V. Ravetch, P. D. Bieniasz, R. A. Bowen, M. C.  
534 Nussenzweig, T. P. Sheahan, Antibody potency, effector function, and  
535 combinations in protection and therapy for SARS-CoV-2 infection in vivo. *J Exp*  
536 *Med* **218**, (2021).
- 537 17. C. E. Z. Chan, S. G. K. Seah, D. H. Chye, S. Massey, M. Torres, A. P. C. Lim,  
538 S. K. K. Wong, J. J. Y. Neo, P. S. Wong, J. H. Lim, G. S. L. Loh, D. L. Wang, J.  
539 D. Boyd-Kirkup, S. Guan, D. Thakkar, G. H. Teo, K. Purushotorman, P. E.  
540 Hutchinson, B. E. Young, D. C. Lye, J. G. Low, P. A. MacAry, H. Hentze, V. S.  
541 Prativadibhayankara, K. Ethirajulu, D. O'Connell, J. Comer, C.-T. K. Tseng, A.  
542 D. T. Barrett, P. J. Ingram, T. Brasel, B. J. Hanson, The Fc-mediated effector  
543 functions of a potent SARS-CoV-2 neutralizing antibody, SC31, isolated from

- 544 an early convalescent COVID-19 patient, are essential for the optimal  
545 therapeutic efficacy of the antibody. *bioRxiv*, 2020.2010.2026.355107 (2020).
- 546 18. H. Natarajan, A. R. Crowley, S. E. Butler, S. Xu, J. A. Weiner, E. M. Bloch, K.  
547 Littlefield, W. Wieland-Alter, R. I. Connor, P. F. Wright, S. E. Benner, T. S.  
548 Bonny, O. Laeyendecker, D. J. Sullivan, S. Shoham, T. Quinn, H. B. Larman,  
549 A. Casadevall, A. Pekosz, A. Redd, A. A. Tobian, M. E. Ackerman, SARS-CoV-  
550 2 antibody signatures robustly predict diverse antiviral functions relevant for  
551 convalescent plasma therapy. *medRxiv*, 2020.2009.2016.20196154 (2020).
- 552 19. J. Dufloo, L. Grzelak, I. Staropoli, Y. Madec, L. Tondeur, F. Anna, S. Pelleau,  
553 A. Wiedemann, C. Planchais, J. Buchrieser, R. Robinot, M.-N. Ungeheuer, H.  
554 Mouquet, P. Charneau, M. White, Y. Lévy, B. Hoen, A. Fontanet, O. Schwartz,  
555 T. Bruel, Asymptomatic and symptomatic SARS-CoV-2 infections elicit  
556 polyfunctional antibodies. *medRxiv*, 2020.2011.2012.20230508 (2020).
- 557 20. B. D. Wines, H. A. Vandervan, S. E. Esparon, A. B. Kristensen, S. J. Kent, P.  
558 M. Hogarth, Dimeric Fcγ<sub>2</sub> Ectodomains as Probes of the Fc Receptor  
559 Function of Anti-Influenza Virus IgG. *J Immunol* **197**, 1507-1516 (2016).
- 560 21. F. Ana-Sosa-Batiz, A. P. R. Johnston, P. M. Hogarth, B. D. Wines, I. Barr, A. K.  
561 Wheatley, S. J. Kent, Antibody-dependent phagocytosis (ADP) responses  
562 following trivalent inactivated influenza vaccination of younger and older adults.  
563 *Vaccine* **35**, 6451-6458 (2017).
- 564 22. F. Yasui, M. Kohara, M. Kitabatake, T. Nishiwaki, H. Fujii, C. Tateno, M. Yoneda,  
565 K. Morita, K. Matsushima, S. Koyasu, C. Kai, Phagocytic cells contribute to the  
566 antibody-mediated elimination of pulmonary-infected SARS coronavirus.  
567 *Virology* **454-455**, 157-168 (2014).
- 568 23. M. E. Ackerman, B. Moldt, R. T. Wyatt, A. S. Dugast, E. McAndrew, S. Tsoukas,  
569 S. Jost, C. T. Berger, G. Sciaranghella, Q. Liu, D. J. Irvine, D. R. Burton, G.  
570 Alter, A robust, high-throughput assay to determine the phagocytic activity of  
571 clinical antibody samples. *J Immunol Methods* **366**, 8-19 (2011).
- 572 24. P. V. Beum, D. A. Mack, A. W. Pawluczkwycz, M. A. Lindorfer, R. P. Taylor,  
573 Binding of Rituximab, Trastuzumab, Cetuximab, or mAb T101 to Cancer Cells  
574 Promotes Trogocytosis Mediated by THP-1 Cells and Monocytes. *The Journal*  
575 *of Immunology* **181**, 8120-8132 (2008).
- 576 25. S. Daubeuf, M. A. Lindorfer, R. P. Taylor, E. Joly, D. Hudrisier, The Direction of  
577 Plasma Membrane Exchange between Lymphocytes and Accessory Cells by  
578 Trogocytosis Is Influenced by the Nature of the Accessory Cell. *The Journal of*  
579 *Immunology* **184**, 1897-1908 (2010).
- 580 26. S. I. Richardson, C. Crowther, N. N. Mkhize, L. Morris, Measuring the ability of  
581 HIV-specific antibodies to mediate trogocytosis. *J Immunol Methods* **463**, 71-  
582 83 (2018).
- 583 27. K. W. Ng, N. Faulkner, G. H. Cornish, A. Rosa, R. Harvey, S. Hussain, R. Ulferts,  
584 C. Earl, A. G. Wrobel, D. J. Benton, C. Roustan, W. Bolland, R. Thompson, A.  
585 Agua-Doce, P. Hobson, J. Heaney, H. Rickman, S. Paraskevopoulou, C. F.  
586 Houlihan, K. Thomson, E. Sanchez, G. Y. Shin, M. J. Spyer, D. Joshi, N.  
587 O'Reilly, P. A. Walker, S. Kjaer, A. Riddell, C. Moore, B. R. Jebson, M.  
588 Wilkinson, L. R. Marshall, E. C. Rosser, A. Radziszewska, H. Peckham, C.  
589 Ciurtin, L. R. Wedderburn, R. Beale, C. Swanton, S. Gandhi, B. Stockinger, J.  
590 McCauley, S. J. Gamblin, L. E. McCoy, P. Cherepanov, E. Nastouli, G.  
591 Kassiotis, Preexisting and de novo humoral immunity to SARS-CoV-2 in  
592 humans. *Science*, eabe1107 (2020).

- 593 28. G. Song, W.-t. He, S. Callaghan, F. Anzanello, D. Huang, J. Ricketts, J. L.  
594 Torres, N. Beutler, L. Peng, S. Vargas, J. Cassell, M. Parren, L. Yang, C.  
595 Ignacio, D. M. Smith, J. E. Voss, D. Nemazee, A. B. Ward, T. Rogers, D. R.  
596 Burton, R. Andrabi, Cross-reactive serum and memory B cell responses to  
597 spike protein in SARS-CoV-2 and endemic coronavirus infection. *bioRxiv*,  
598 2020.2009.2022.308965 (2020).
- 599 29. T. Aydillo, A. Rombauts, D. Stadlbauer, S. Aslam, G. Abelenda-Alonso, A.  
600 Escalera, F. Amanat, K. Jiang, F. Krammer, J. Carratala, A. García-Sastre,  
601 Antibody Immunological Imprinting on COVID-19 Patients. *medRxiv*,  
602 2020.2010.2014.20212662 (2020).
- 603 30. B. M. Westerhuis, M. Aguilar-Bretones, M. P. Raadsen, E. de Bruin, N. M. A.  
604 Okba, B. L. Haagmans, T. Langerak, H. Endeman, J. P. C. van den Akker, D.  
605 A. M. P. J. Gommers, E. C. M. van Gorp, B. H. G. Rockx, M. P. G. Koopmans,  
606 G. P. van Nierop, Severe COVID-19 patients display a back boost of seasonal  
607 coronavirus-specific antibodies. *medRxiv*, 2020.2010.2010.20210070 (2020).
- 608 31. T. Zohar, C. Loos, S. Fischinger, C. Atyeo, C. Wang, M. D. Slein, J. Burke, J.  
609 Yu, J. Feldman, B. M. Hauser, T. Caradonna, A. G. Schmidt, Y. Cai, H. Streeck,  
610 E. T. Ryan, D. H. Barouch, R. C. Charles, D. A. Lauffenburger, G. Alter,  
611 Compromised Humoral Functional Evolution Tracks with SARS-CoV-2  
612 Mortality. *Cell*, (2020).
- 613 32. R. Gasser, M. Cloutier, J. Prévost, C. Fink, É. Ducas, S. Ding, N. Dussault, P.  
614 Landry, T. Tremblay, A. Laforce-Lavoie, A. Lewin, G. Beaudoin-Bussièrès, A.  
615 Laumaea, H. Medjahed, C. Larochelle, J. Richard, G. A. Dekaban, J. D.  
616 Dikeakos, R. Bazin, A. Finzi, Major role of IgM in the neutralizing activity of  
617 convalescent plasma against SARS-CoV-2. *bioRxiv*, 2020.2010.2009.333278  
618 (2020).
- 619 33. Z. Wang, J. C. C. Lorenzi, F. Muecksch, S. Finkin, C. Viant, C. Gaebler, M.  
620 Cipolla, H.-H. Hoffmann, T. Y. Oliveira, D. A. Oren, V. Ramos, L. Nogueira, E.  
621 Michailidis, D. F. Robbiani, A. Gazumyan, C. M. Rice, T. Hatzioannou, P. D.  
622 Bieniasz, M. Caskey, M. C. Nussenzweig, Enhanced SARS-CoV-2  
623 neutralization by dimeric IgA. *Science Translational Medicine*, eabf1555 (2020).
- 624 34. D. Sterlin, A. Mathian, M. Miyara, A. Mohr, F. Anna, L. Claër, P. Quentric, J.  
625 Fadlallah, H. Devilliers, P. Ghillani, C. Gunn, R. Hockett, S. Mudumba, A.  
626 Guihot, C.-E. Luyt, J. Mayaux, A. Beurton, S. Fourati, T. Bruel, O. Schwartz, J.-  
627 M. Lacorte, H. Yssel, C. Parizot, K. Dorgham, P. Charneau, Z. Amoura, G.  
628 Gorochov, IgA dominates the early neutralizing antibody response to SARS-  
629 CoV-2. *Science Translational Medicine*, eabd2223 (2020).
- 630 35. W. He, C. J. Chen, C. E. Mullarkey, J. R. Hamilton, C. K. Wong, P. E. Leon, M.  
631 B. Uccellini, V. Chromikova, C. Henry, K. W. Hoffman, J. K. Lim, P. C. Wilson,  
632 M. S. Miller, F. Krammer, P. Palese, G. S. Tan, Alveolar macrophages are  
633 critical for broadly-reactive antibody-mediated protection against influenza A  
634 virus in mice. *Nat Commun* **8**, 846 (2017).
- 635 36. J. Zhao, Q. Yuan, H. Wang, W. Liu, X. Liao, Y. Su, X. Wang, J. Yuan, T. Li, J.  
636 Li, S. Qian, C. Hong, F. Wang, Y. Liu, Z. Wang, Q. He, Z. Li, B. He, T. Zhang,  
637 Y. Fu, S. Ge, L. Liu, J. Zhang, N. Xia, Z. Zhang, Antibody responses to SARS-  
638 CoV-2 in patients of novel coronavirus disease 2019. *Clin Infect Dis*, (2020).
- 639 37. K. Duan, B. Liu, C. Li, H. Zhang, T. Yu, J. Qu, M. Zhou, L. Chen, S. Meng, Y.  
640 Hu, C. Peng, M. Yuan, J. Huang, Z. Wang, J. Yu, X. Gao, D. Wang, X. Yu, L.  
641 Li, J. Zhang, X. Wu, B. Li, Y. Xu, W. Chen, Y. Peng, Y. Hu, L. Lin, X. Liu, S.  
642 Huang, Z. Zhou, L. Zhang, Y. Wang, Z. Zhang, K. Deng, Z. Xia, Q. Gong, W.



- 643 Zhang, X. Zheng, Y. Liu, H. Yang, D. Zhou, D. Yu, J. Hou, Z. Shi, S. Chen, Z.  
644 Chen, X. Zhang, X. Yang, Effectiveness of convalescent plasma therapy in  
645 severe COVID-19 patients. *Proc Natl Acad Sci U S A* **117**, 9490-9496 (2020).
- 646 38. M. J. Joyner, R. S. Wright, D. Fairweather, J. W. Senefeld, K. A. Bruno, S. A.  
647 Klassen, R. E. Carter, A. M. Klompas, C. C. Wiggins, J. R. Shepherd, R. F. Rea,  
648 E. R. Whelan, A. J. Clayburn, M. R. Spiegel, P. W. Johnson, E. R. Lesser, S.  
649 E. Baker, K. F. Larson, J. G. Ripoll, K. J. Andersen, D. O. Hodge, K. L. Kunze,  
650 M. R. Buras, M. N. Vogt, V. Herasevich, J. J. Dennis, R. J. Regimbal, P. R.  
651 Bauer, J. E. Blair, C. M. van Buskirk, J. L. Winters, J. R. Stubbs, N. S. Paneth,  
652 N. C. Verdun, P. Marks, A. Casadevall, Early safety indicators of COVID-19  
653 convalescent plasma in 5,000 patients. *J Clin Invest*, (2020).
- 654 39. C. Shen, Z. Wang, F. Zhao, Y. Yang, J. Li, J. Yuan, F. Wang, D. Li, M. Yang, L.  
655 Xing, J. Wei, H. Xiao, Y. Yang, J. Qu, L. Qing, L. Chen, Z. Xu, L. Peng, Y. Li,  
656 H. Zheng, F. Chen, K. Huang, Y. Jiang, D. Liu, Z. Zhang, Y. Liu, L. Liu,  
657 Treatment of 5 Critically Ill Patients With COVID-19 With Convalescent Plasma.  
658 *JAMA*, (2020).
- 659 40. A. Agarwal, A. Mukherjee, G. Kumar, P. Chatterjee, T. Bhatnagar, P. Malhotra,  
660 Convalescent plasma in the management of moderate covid-19 in adults in  
661 India: open label phase II multicentre randomised controlled trial (PLACID Trial).  
662 *BMJ* **371**, m3939 (2020).
- 663 41. L. Li, W. Zhang, Y. Hu, X. Tong, S. Zheng, J. Yang, Y. Kong, L. Ren, Q. Wei,  
664 H. Mei, C. Hu, C. Tao, R. Yang, J. Wang, Y. Yu, Y. Guo, X. Wu, Z. Xu, L. Zeng,  
665 N. Xiong, L. Chen, J. Wang, N. Man, Y. Liu, H. Xu, E. Deng, X. Zhang, C. Li, C.  
666 Wang, S. Su, L. Zhang, J. Wang, Y. Wu, Z. Liu, Effect of Convalescent Plasma  
667 Therapy on Time to Clinical Improvement in Patients With Severe and Life-  
668 threatening COVID-19: A Randomized Clinical Trial. *JAMA*, (2020).
- 669 42. V. A. Simonovich, L. D. Burgos Pratx, P. Scibona, M. V. Beruto, M. G. Vallone,  
670 C. Vázquez, N. Savoy, D. H. Giunta, L. G. Pérez, M. d. L. Sánchez, A. V.  
671 Gamarnik, D. S. Ojeda, D. M. Santoro, P. J. Camino, S. Antelo, K. Rainero, G.  
672 P. Vidiella, E. A. Miyazaki, W. Cornistein, O. A. Trabadelo, F. M. Ross, M. Spotti,  
673 G. Funtowicz, W. E. Scordo, M. H. Losso, I. Ferniot, P. E. Pardo, E. Rodriguez,  
674 P. Rucci, J. Pasquali, N. A. Fuentes, M. Esperatti, G. A. Speroni, E. C. Nannini,  
675 A. Matteaccio, H. G. Michelangelo, D. Follmann, H. C. Lane, W. H. Belloso, A  
676 Randomized Trial of Convalescent Plasma in Covid-19 Severe Pneumonia.  
677 *New England Journal of Medicine*, (2020).
- 678 43. S. Chakraborty, J. Gonzalez, K. Edwards, V. Mallajosyula, A. S. Buzzanco, R.  
679 Sherwood, C. Buffone, N. Kathale, S. Providenza, M. M. Xie, J. R. Andrews, C.  
680 A. Blish, U. Singh, H. Dugan, P. C. Wilson, T. D. Pham, S. D. Boyd, K. C.  
681 Nadeau, B. A. Pinsky, S. Zhang, M. J. Memoli, J. K. Taubenberger, T. Morales,  
682 J. M. Schapiro, G. S. Tan, P. Jagannathan, T. T. Wang, Proinflammatory IgG  
683 Fc structures in patients with severe COVID-19. *Nature Immunology*, (2020).
- 684 44. W. Hoepel, H.-J. Chen, S. Allahverdiyeva, X. Manz, J. Aman, P. Bonta, P.  
685 Brouwer, S. de Taeye, T. Caniels, K. van der Straten, K. Golebski, G. Griffith,  
686 R. Jonkers, M. Larsen, F. Linty, A. Neele, J. Nouta, F. van Baarle, C. van  
687 Drunen, A. Vlaar, G. de Bree, R. Sanders, L. Willemsen, M. Wuhrer, H. J.  
688 Bogaard, M. van Gils, G. Vidarsson, M. de Winther, J. den Dunnen, Anti-SARS-  
689 CoV-2 IgG from severely ill COVID-19 patients promotes macrophage hyper-  
690 inflammatory responses. *bioRxiv*, 2020.2007.2013.190140 (2020).
- 691 45. F. P. Polack, M. N. Teng, P. L. Collins, G. A. Prince, M. Exner, H. Regele, D.  
692 D. Lirman, R. Rabold, S. J. Hoffman, C. L. Karp, S. R. Kleeberger, M. Wills-

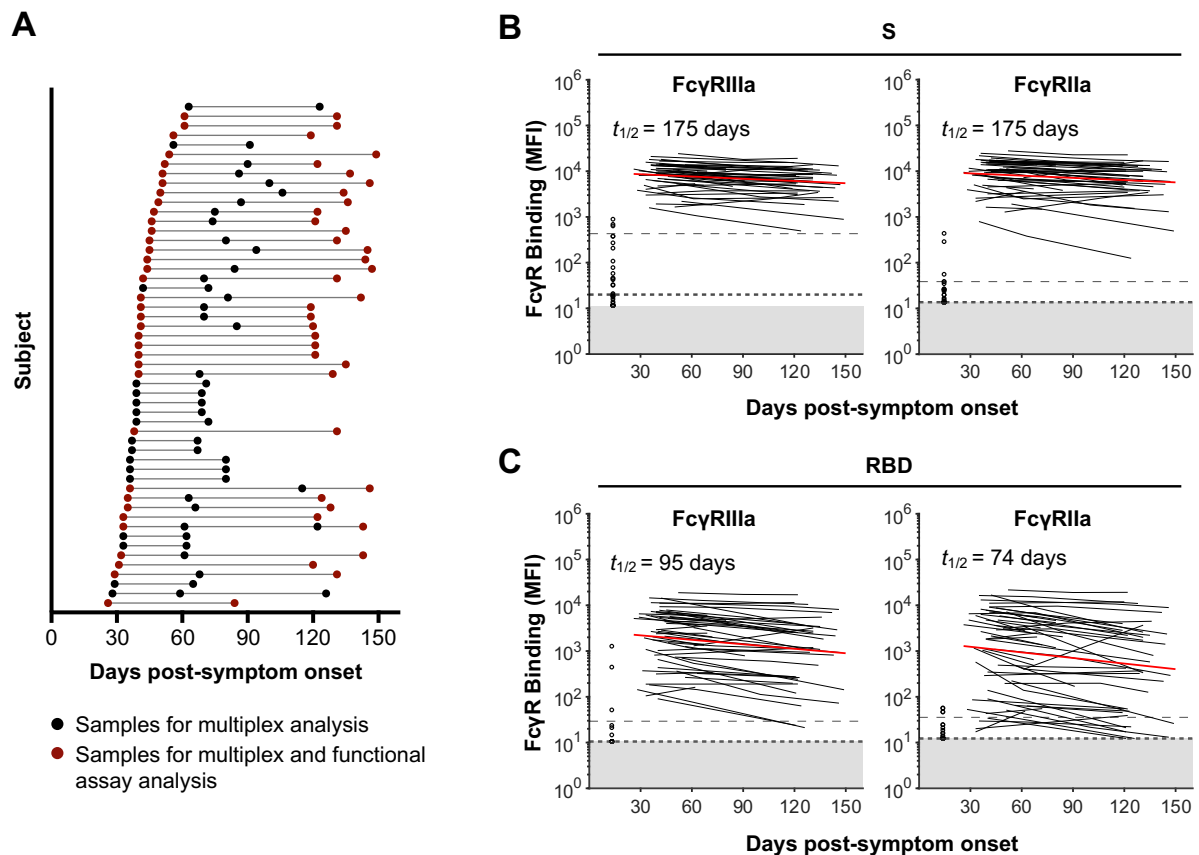
- 693 Karp, R. A. Karron, A role for immune complexes in enhanced respiratory  
694 syncytial virus disease. *J Exp Med* **196**, 859-865 (2002).
- 695 46. F. P. Polack, Atypical measles and enhanced respiratory syncytial virus  
696 disease (ERD) made simple. *Pediatr Res* **62**, 111-115 (2007).
- 697 47. R. L. Tillett, J. R. Sevinsky, P. D. Hartley, H. Kerwin, N. Crawford, A. Gorzalski,  
698 C. Laverdure, S. C. Verma, C. C. Rossetto, D. Jackson, M. J. Farrell, S. Van  
699 Hooser, M. Pandori, Genomic evidence for reinfection with SARS-CoV-2: a  
700 case study. *The Lancet Infectious Diseases*.
- 701 48. B. Prado-Vivar, M. Becerra-Wong, J. J. Guadalupe, S. Marquez, B. Gutierrez,  
702 P. Rojas-Silva, M. Grunauer, G. Trueba, V. Barragan, P. Cardenas, COVID-19  
703 Re-Infection by a Phylogenetically Distinct SARS-CoV-2 Variant, First  
704 Confirmed Event in South America. *SSRN*, (2020).
- 705 49. K. J. Selva, C. E. van de Sandt, M. M. Lemke, C. Y. Lee, S. K. Shoffner, B. Y.  
706 Chua, T. H. O. Nguyen, L. C. Rowntree, L. Hensen, M. Koutsakos, C. Y. Wong,  
707 D. C. Jackson, K. L. Flanagan, J. Crowe, A. C. Cheng, D. L. Doolan, F. Amanat,  
708 F. Krammer, K. Chappell, N. Modhiran, D. Watterson, P. Young, B. Wines, P.  
709 M. Hogarth, R. Esterbauer, H. G. Kelly, H.-X. Tan, J. A. Juno, A. K. Wheatley,  
710 S. J. Kent, K. B. Arnold, K. Kedzierska, A. W. Chung, Distinct systems serology  
711 features in children, elderly and COVID patients. *medRxiv*,  
712 2020.2005.2011.20098459 (2020).
- 713 50. B. D. Wines, H. M. Trist, R. C. Monteiro, C. Van Kooten, P. M. Hogarth, Fc  
714 receptor gamma chain residues at the interface of the cytoplasmic and  
715 transmembrane domains affect association with Fc $\alpha$ RI, surface expression,  
716 and function. *J Biol Chem* **279**, 26339-26345 (2004).
- 717 51. P. A. Darrah, D. T. Patel, P. M. De Luca, R. W. Lindsay, D. F. Davey, B. J.  
718 Flynn, S. T. Hoff, P. Andersen, S. G. Reed, S. L. Morris, M. Roederer, R. A.  
719 Seder, Multifunctional TH1 cells define a correlate of vaccine-mediated  
720 protection against *Leishmania major*. *Nat Med* **13**, 843-850 (2007).
- 721

## 722 **Acknowledgments**

723 We thank the cohort participants for generously providing samples. We thank  
724 Francesca Mordant and Kanta Subbarao (University of Melbourne) for performing the  
725 SARS-CoV-2 neutralisation assays. We acknowledge the Melbourne Cytometry  
726 Platform for provision of flow cytometry services. The following reagent was produced  
727 under HHSN272201400008C and obtained through BEI Resources, NIAID, NIH:  
728 Spike Glycoprotein Receptor Binding Domain (RBD) from SARS-Related Coronavirus  
729 2, Wuhan-Hu-1 with C-Terminal Histidine Tag, Recombinant from HEK293F Cells,  
730 NR-52366. This study was supported by the Victorian Government, an Australian  
731 government Medical Research Future Fund award GNT2002073 (SJK, MPD, and  
732 AKW), the ARC Centre of Excellence in Convergent Bio-Nano Science and  
733 Technology (SJK), an NHMRC program grant APP1149990 (SJK and MPD), NHMRC  
734 project grants GNT1162760 (AKW), GNT1145303 (PMH and BDW), an NHMRC-EU  
735 collaborative award APP1115828 (SJK and MPD), the European Union Horizon 2020  
736 Research and Innovation Programme under grant agreement 681137 (SJK), and  
737 Emergent Ventures Fast Grants (AWC). JAJ, AWC and SJK are supported by NHMRC  
738 fellowships. AKW, DC and MPD are supported by NHMRC Investigator grants.  
739 Figures were created using BioRender.

740

741 **Figures**



742

743 **Fig. 1. Dynamics of SARS-CoV-2 S and RBD-specific dimeric FcγR-binding**

744 **antibodies in COVID-19 convalescent individuals. (A)** Timeline of sample

745 collection for each COVID-19 convalescent subject (n=53). Subjects with 2 samples

746 at least 60 days apart were chosen for functional assay analysis (n=36). **(B-C)** Kinetics

747 of SARS-CoV-2 S and RBD-specific dimeric FcγRIIIa (V158) and dimeric FcγRIIa

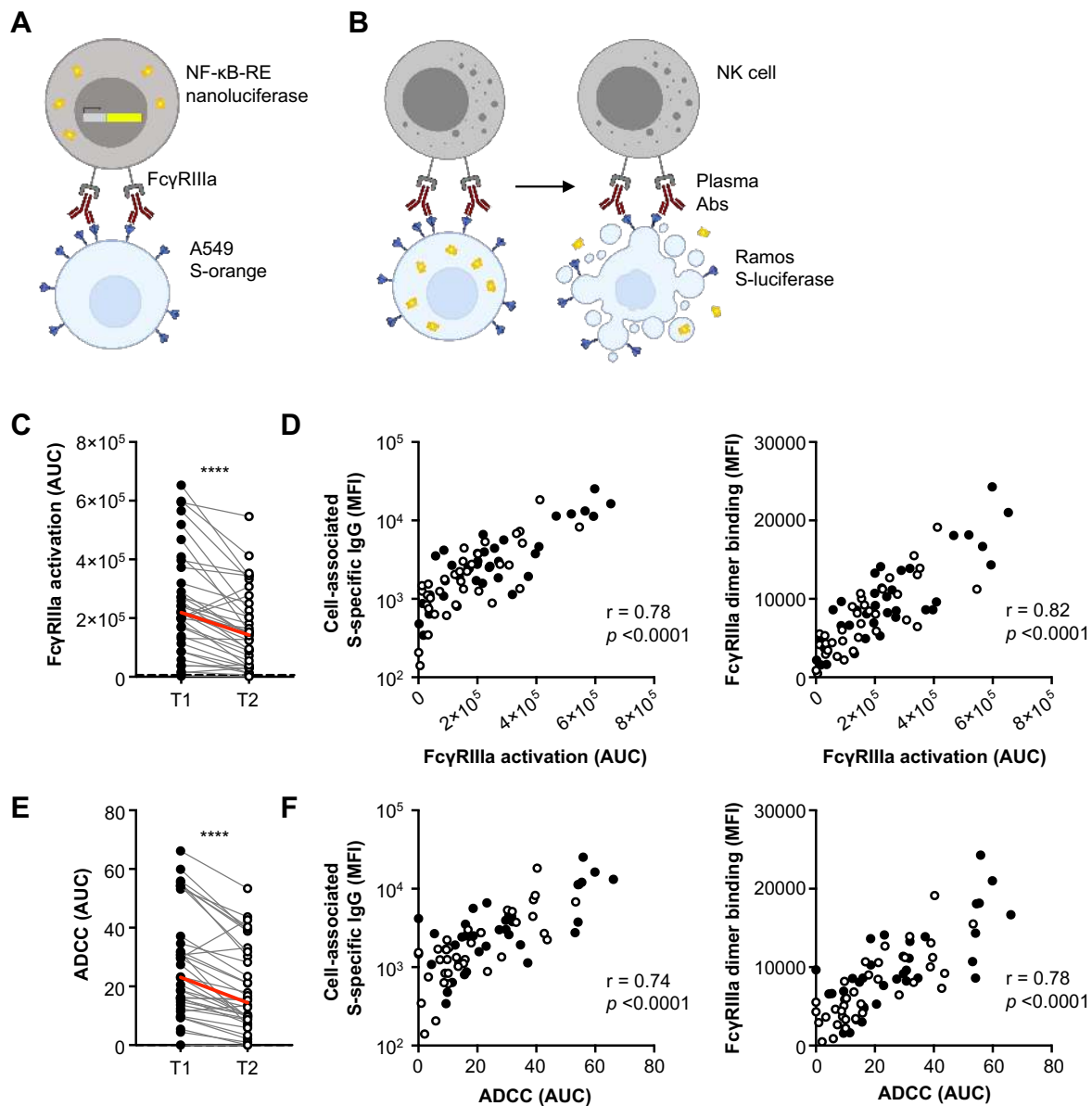
748 (H131) binding antibodies over time. The best-fit decay slopes (red lines) and

749 estimated half-lives ( $t_{1/2}$ ) are indicated for COVID-19 convalescent individuals.

750 Uninfected controls (n=33) are shown in open circles, with the median and 90%

751 percentile responses presented as thick and thin dashed lines respectively. The limit

752 of detection is shown as the shaded area.



753

754 **Fig. 2. ADCC responses in COVID-19 convalescent individuals over time. (A)**

755 Schematic of the FcγRIIIa NF-κB activation assay. IIA1.6 cells expressing FcγRIIIa

756 V158 and a NF-κB response element-driven nanoluciferase reporter were co-

757 incubated with A549 S-orange target cells and plasma from COVID-19 convalescent

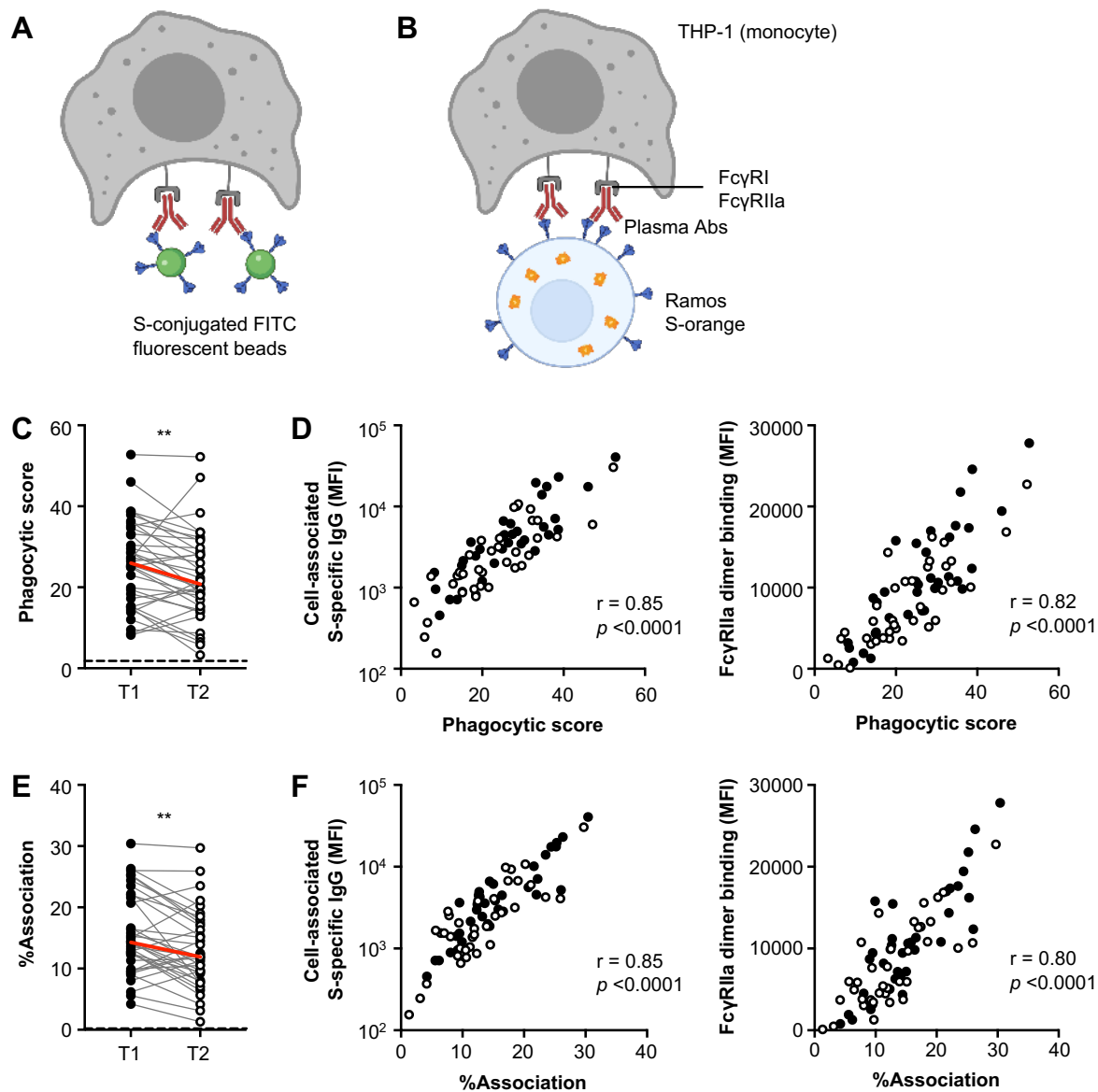
758 individuals or uninfected controls. The engagement of FcγRIIIa by S-specific

759 antibodies activates downstream NF-κB signalling and nano-luciferase expression. **(B)**

760 Schematic of the luciferase-based ADCC assay. Purified NK cells from healthy donors

761 were co-incubated with Ramos S-luciferase target cells and plasma. ADCC is

762 measured as the loss of cellular luciferase. **(C)** S-specific FcγRIIIa-activating plasma  
763 antibodies in COVID-19 convalescent individuals in the first (T1; filled) and last (T2;  
764 open) timepoints available. **(D)** Correlation of S-specific FcγRIIIa-activating antibodies  
765 to cell-associated S-specific IgG and S-specific dimeric FcγRIIIa-binding antibodies.  
766 **(E)** S-specific ADCC mediated by plasma antibodies from COVID-19 convalescent  
767 individuals in the first (T1; filled) and last (T2; open) timepoints available. **(F)**  
768 Correlation of S-specific ADCC to cell-associated S-specific IgG and S-specific  
769 dimeric FcγRIIIa-binding antibodies. Red lines indicate the median responses of  
770 COVID-19 convalescent individuals (N=36) while dashed lines indicate median  
771 responses of uninfected controls (N=8). Statistical analyses were performed with the  
772 Wilcoxon signed-rank test (\*\*\*\*,  $p < 0.0001$ ). Correlations were performed with the non-  
773 parametric Spearman test.



774

775

776 **Fig. 3. ADP responses in COVID-19 convalescent individuals over time. (A)**

777 Schematic of the bead-based ADP assay. THP-1 cells were incubated with S-

778 conjugated fluorescent beads and plasma from COVID-19 convalescent individuals or

779 uninfected controls. The uptake of fluorescent beads was measured by flow cytometry

780 **(B)** Schematic of the THP-1 Fc $\gamma$ R-dependent cell association assay. Ramos S-orange

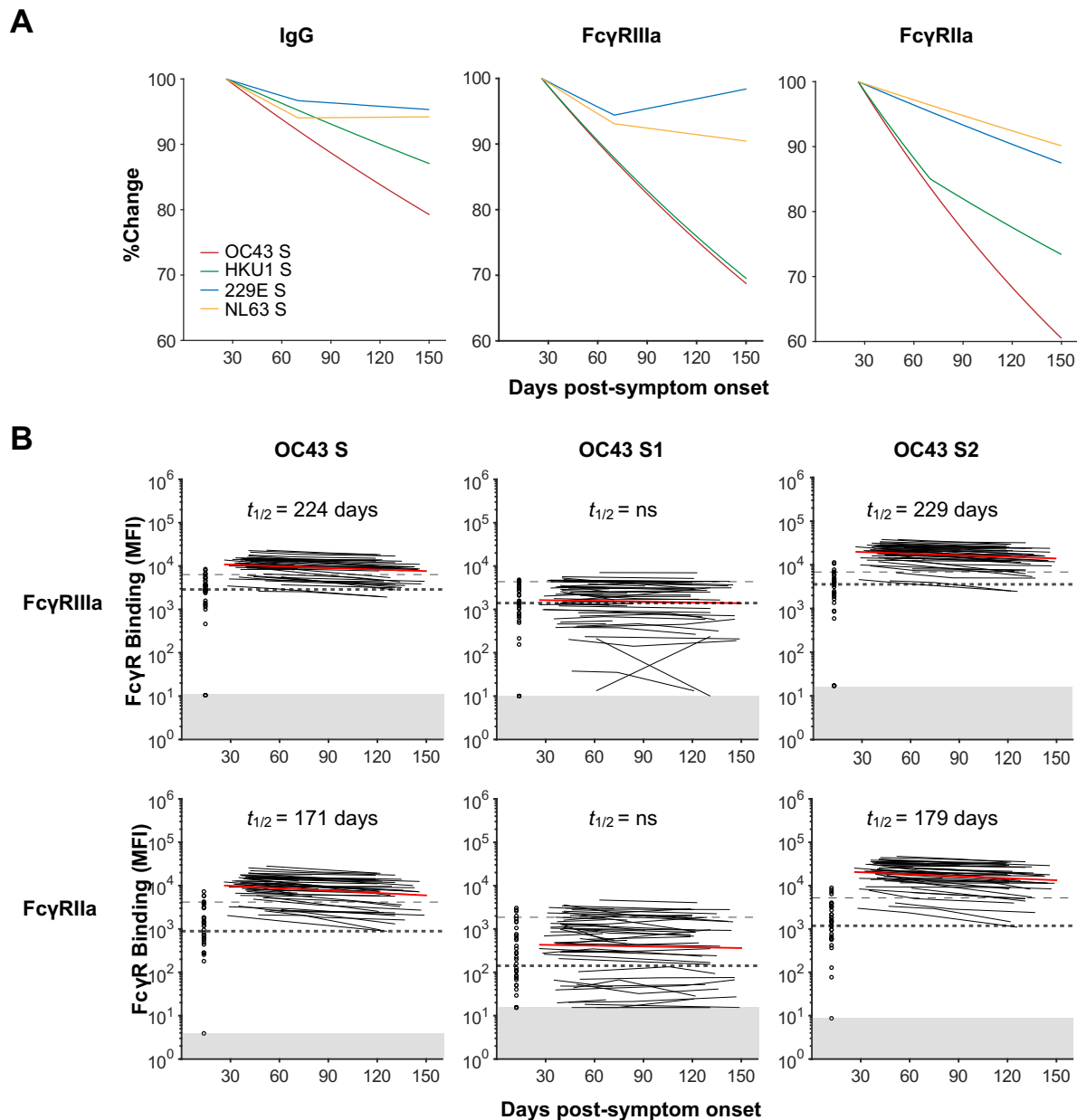
781 cells were pre-incubated with plasma prior to co-incubation with THP-1 cells. The

782 association of THP-1 cells with Ramos S-orange cells was measured by flow

783 cytometry. **(C)** ADP of S-conjugated beads mediated by plasma antibodies from

784 COVID-19 convalescent individuals in the first (T1) and last (T2) timepoints available.  
785 **(D)** Correlation of ADP to cell-associated S-specific IgG and S-specific dimeric  
786 FcγRIIIa-binding antibodies. **(E)** FcγR-dependent association of THP-1 cells with  
787 Ramos S-orange cells mediated by plasma antibodies from COVID-19 convalescent  
788 individuals in the first (T1) and last (T2) timepoints available. **(F)** Correlation of  
789 association of THP-1 cells with Ramos S-orange cells to cell-associated S-specific IgG  
790 and S-specific dimeric FcγRIIIa-binding antibodies. Red lines indicate the median  
791 responses of COVID-19 convalescent individuals (N=36) while dashed lines indicate  
792 median responses of uninfected controls (N=8). Statistical analyses were performed  
793 with the Wilcoxon signed-rank test (\*\*,  $p < 0.01$ ). Correlations were performed with the  
794 non-parametric Spearman test.





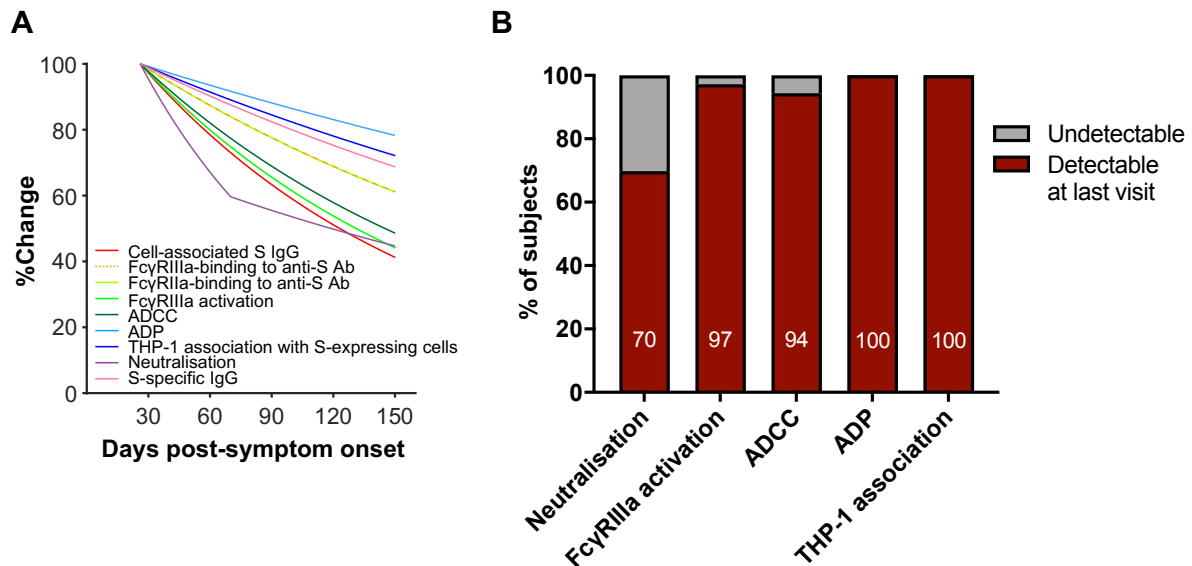
795  
796

797 **Fig. 4. Dynamics of HCoV S-specific antibodies in COVID-19 convalescent**  
 798 **individuals. (A)** Best fit decay slopes of IgG and dimeric FcγR-binding antibodies  
 799 against S from HCoV strains OC43, HKU1, 229E and NL63. The responses at  
 800 timepoint 1 for each parameter are set to 100% and the %change over time is shown.  
 801 **(B-C)** Kinetics of dimeric FcγRIIIa (V158) and FcγRIIa (H131) binding antibodies  
 802 against HCoV-OC43 S antigens over time in COVID-19 convalescent individuals  
 803 (n=53). The best-fit decay slopes (red lines) and estimated half-lives ( $t_{1/2}$ ) are indicated

804 for COVID-19 convalescent individuals. Uninfected controls (n=33) are shown in open  
805 circles, with the median and 90% percentile responses presented as thick and thin  
806 dashed lines respectively. The limit of detection is shown as the shaded area.

807

808



809  
810

811 **Fig. 5. Decay kinetics of binding antibodies, neutralisation and Fc effector**  
812 **functions following SARS-CoV-2 infection. (A)** Best fit decay slopes of various  
813 antibody parameters against SARS-CoV-2 S over time. The responses at timepoint 1  
814 for each parameter are set to 100% and the %change over time is shown. **(B)** The  
815 percentage of subjects having detectable responses above (red) and below (grey)  
816 background levels at the last visit are shown. Background levels for each assay were  
817 the median responses of uninfected controls.

818



Minerva Access is the Institutional Repository of The University of Melbourne

**Author/s:**

Lee, WS;Selva, KJ;Davis, S;Wines, B;Reynaldi, A;Esterbauer, R;Kelly, H;Haycroft, E;Tan, H-X;Juno, J;Wheatley, A;Hogarth, M;Cromer, D;Davenport, M;Chung, A;Kent, S

**Title:**

Decay of Fc-dependent antibody functions after mild to moderate COVID-19

**Date:**

2020-12-14

**Citation:**

Lee, W. S., Selva, K. J., Davis, S., Wines, B., Reynaldi, A., Esterbauer, R., Kelly, H., Haycroft, E., Tan, H. -X., Juno, J., Wheatley, A., Hogarth, M., Cromer, D., Davenport, M., Chung, A. & Kent, S. (2020). Decay of Fc-dependent antibody functions after mild to moderate COVID-19. medRxiv, <https://doi.org/10.1101/2020.12.13.20248143>.

**Persistent Link:**

<http://hdl.handle.net/11343/278511>

**License:**

[CC BY-NC-ND](#)